

Distilling Formal Logic into Neural Spaces: A Kernel Alignment Approach for Signal Temporal Logic

Sara Candussio

AILab, MIGe, University of Trieste, IT

SARA.CANDUSSIO@PHD.UNITS.IT

Gabriele Sarti

Khoury College of Computing Sciences, Northeastern University, Boston, MA, USA

G.SARTI@NORTHEASTERN.EDU

Gaia Saveri

AILab, MIGe, University of Trieste, IT

GAIA.SAVERI@PHD.UNITS.IT

Luca Bortolussi

AILab, MIGe, University of Trieste, IT

LBORTOLUSSI@UNITS.IT

Editor: Under Review for NeSy 2026

Abstract

We introduce a framework for learning continuous neural representations of formal specifications by distilling the geometry of their semantics into a latent space. Existing approaches rely either on symbolic kernels – which preserve behavioural semantics but are computationally prohibitive, anchor-dependent, and non-invertible – or on syntax-based neural embeddings that fail to capture underlying structures. Our method bridges this gap: using a teacher-student setup, we distill a symbolic robustness kernel into a Transformer encoder. Unlike standard contrastive methods, we supervise the model with a continuous, kernel-weighted geometric alignment objective that penalizes errors in proportion to their semantic discrepancies. Once trained, the encoder produces embeddings in a single forward pass, effectively mimicking the kernel’s logic at a fraction of its computational cost. We apply our framework to Signal Temporal Logic (STL), demonstrating that the resulting neural representations faithfully preserve the semantic similarity of STL formulae, accurately predict robustness and constraint satisfaction, and remain intrinsically invertible. Our proposed approach enables highly efficient, scalable neuro-symbolic reasoning and formula reconstruction without repeated kernel computation at runtime.

1. Introduction

Formal specification languages such as *Signal Temporal Logic* (STL, [Maler and Ničković, 2004](#)) are central to the analysis and control of cyber-physical systems, enabling the formalization of safety, liveness, and performance requirements over time-varying signals. Recent work integrates STL within machine learning pipelines ([Raman et al., 2015](#); [Bombara and Belta, 2021](#); [Akazaki et al., 2018](#); [Li et al., 2017](#); [Hasanbeig et al., 2020](#)), supporting tasks such as requirement mining, specification-guided learning, and neural verification. STL admits a quantitative semantics via robustness ([Fainekos and Pappas, 2006](#)), which measures the degree to which a formula is satisfied or violated. Robustness-based kernel methods offer a semantic alternative: formulae are compared by computing their robustness over a distribution of signals ([Bortolussi et al., 2022](#)), embedding specifications into a Hilbert space where distance reflects behavioural agreement rather than syntax ([Saveri et al., 2024](#)). However, estimating pairwise similarities requires repeated robustness evaluations and scales

quadratically in the number of formulae. Moreover, behaviourally equivalent but lexically distinct specifications collapse to the same point, making the mapping non-invertible. While acceptable for similarity estimation, this is problematic when generating or manipulating a large number of formulae. While neural reconstruction from kernel embeddings has been explored (Candussio et al., 2025), generalizing these results depends critically on the coverage of the formulae reference sets selected for model training.

Recent works explore using Transformers-based neural encoders to embed formulae in a shared vector space, producing representations that can be computed efficiently through a single forward pass (Allamanis et al., 2018; Feng et al., 2020; Dong et al., 2021; Reimers and Gurevych, 2019). However, most existing approaches rely primarily on lexical similarity (Gao et al., 2022), resulting in embeddings that fail to fully capture the complex semantic relationships underlying formal language specifications.

We bridge these paradigms by training a neural encoder to approximate the geometry induced by the STL semantic kernel. Treating the kernel as a teacher metric, we cast representation learning as a relational distillation process (Hinton et al., 2015; Park et al., 2019), aligning embedding inner products with kernel robustness-based similarities. A Transformer encoder is trained with pairwise kernel similarities using a *weighted geometric alignment objective* that emphasizes corrections for large semantic discrepancies. The cost of robustness computation is thus front-loaded during training, reducing inference costs to a single forward pass with the distilled model, thereby amortizing evaluation computations.

Contributions

1. We propose a procedure to distill STL quantitative semantics into neural embeddings, employing a robustness-based semantic kernel to control the geometry of learned representations. The resulting latent space approximates the associated Reproducing Kernel Hilbert Space (RKHS) (Berlinet and Thomas-Agnan, 2004), organizing formulae by their behavioural semantics.
2. We introduce a weighted pairwise objective that encourages the neural encoder to mimic the kernel similarities. The weighting prioritizes examples where the model deviates most from the kernel signal, ensuring the encoder focuses on its largest errors.

2. Background

2.1. Signal Temporal Logic

Signal Temporal Logic (STL) (Maler and Ničković, 2004) is a linear-time temporal logic for specifying properties of real-valued trajectories over dense time domains. A trajectory (or signal) is a function $\xi : I \rightarrow D$, where $I \subseteq \mathbb{R}_{\geq 0}$ is a time interval and $D \subseteq \mathbb{R}^k$ is the state space. We denote by \mathcal{T} the space of admissible trajectories and by \mathcal{F} the set of well-formed STL formulae. The syntax of STL is given by $\varphi ::= \top \mid \pi \mid \neg\varphi \mid \varphi_1 \wedge \varphi_2 \mid \varphi_1 \mathbf{U}_{[a,b]} \varphi_2$, where π is an atomic predicate of the form $f_\pi(x) \geq 0$, \neg and \wedge are Boolean connectives, and $\mathbf{U}_{[a,b]}$ is the time-bounded until operator, from which the eventually $\mathbf{F}_{[a,b]}\varphi \equiv \top \mathbf{U}_{[a,b]}\varphi$ and always $\mathbf{G}_{[a,b]}\varphi \equiv \neg\mathbf{F}_{[a,b]}\neg\varphi$ operators are derived.

STL admits both Boolean and quantitative semantics (Appendix A); the boolean semantics determines whether a trajectory ξ satisfies a formula φ at time t ; the quantitative

semantics, called *robustness* and denoted $\rho(\varphi, \xi, t) \in \mathbb{R}$, measures the degree of satisfaction or violation at time t . In what follows, when $t = 0$ we use the shortcut notation $\rho(\varphi, \xi)$ to indicate $\rho(\varphi, \xi, 0)$. Positive robustness implies satisfaction, negative robustness implies violation, and the magnitude quantifies the distance from the satisfaction boundary.

2.2. Semantic-preserving embeddings for Signal Temporal Logic

The quantitative semantics enables a functional view of specifications: each formula $\varphi \in \mathcal{F}$ can be interpreted as a real-valued function over trajectories, $\Phi(\varphi) := \rho(\varphi, \cdot)$. Fixing a probability measure μ_0 over \mathcal{T} , this induces the representation $\Phi(\varphi) \in L^2(\mathcal{T}, \mu_0)$ and a semantic similarity measure defined via the inner product:

$$k(\varphi_i, \varphi_j) = \langle \Phi(\varphi_i), \Phi(\varphi_j) \rangle_{\mu_0} = \int_{\mathcal{T}} \rho(\varphi_i, \xi) \rho(\varphi_j, \xi) d\mu_0(\xi). \quad (1)$$

This construction defines a positive-definite kernel over \mathcal{F} and embeds STL specifications into a Reproducing Kernel Hilbert Space (RKHS), where proximity reflects behavioural similarity over the trajectory distribution μ_0 rather than lexical matching.

In practice, the integral is approximated via Monte Carlo sampling over trajectories. Cosine normalization and exponential mappings are typically applied to obtain a scale-invariant RBF kernel (Appendix A). The resulting geometry admits a behavioural interpretation: the distance between the embeddings of two formulae measures disagreement in expected robustness, providing a continuous notion of semantic similarity grounded in system behaviour.

2.3. Kernel embedding inversion and coverage limitations

From the definition of STL kernel (Equation 1), a continuous representation $k(\varphi) \in \mathbb{R}^D$ of a formula $\varphi \in \mathcal{F}$ can be obtained by fixing a (possibly random) set of D *anchor formulae* $\{\varphi_j\}_{j=1}^D$ and devising the vector $k(\varphi) = [k(\varphi, \varphi_j)]_{j=0}^{D-1}$. Then, if we want to map another specification $\varphi' \in \mathcal{F}$ in the same latent space, allowing meaningful comparison of the resulting embeddings, we need to rely on the same anchor set to get $k(\varphi') = [k(\varphi', \varphi_j)]_{j=0}^{D-1}$. Hence, the resulting representation is not intrinsic to the formula itself, but defined in relation to a coordinate system induced by the anchor set. Inverting such robustness-based embeddings has been explored via large-scale nearest-neighbour retrieval over $\sim 10^7$ moderate-complexity formulae (Saveri and Bortolussi, 2024), and Transformer decoders trained on $\sim 10^5$ examples (Candussio et al., 2025). Both approaches rely on a finite anchor set that defines the span of the semantic space they can represent.

2.4. Neural encoders and pooling strategies

In principle, embeddings of symbolic expressions can be learned with neural networks (Alamanis et al., 2018; Feng et al., 2020). A parametric encoder $f_\theta : \mathcal{S} \rightarrow \mathbb{R}^d$ can be trained to map each symbolic object $s \in \mathcal{S}$ to a fixed-dimensional vector. Symbolic expressions can be processed with a Transformer (Vaswani et al., 2017), producing token embeddings that capture both local structure and long-range dependencies. To obtain a single embedding for the entire expression, token-level representations can be aggregated via pooling. Typical

strategies include averaging the token representations (*mean pooling*) or using a designated token representation (e.g., the special start-of-sequence tokens [CLS] and [BOS]), which is explicitly trained to summarize the sequence and capture its global contextual information (Devlin et al., 2019; Radford and Narasimhan, 2018; Reimers and Gurevych, 2019).

3. Related works

3.1. Kernel-guided neural representation learning

Learning neural embeddings that preserve the geometry of a target kernel has been explored under the umbrella of *kernel distillation* and *metric supervision*. In this framework, the kernel defines pairwise similarities between inputs, which the neural encoder is trained to reproduce in its latent space (Park et al., 2019). Representation distillation approaches have been proposed in various domains, e.g., convolutional networks (Jones et al., 2019) and Neural Tangent Kernels (Mahowald et al., 2026). Theoretical analyses indicate that similarity-preserving learning on a hypersphere can approximate the leading eigenspace of a kernel operator (Lee et al., 2025). Continuous kernel similarities thus act as soft supervision, allowing neural encoders to internalize the semantic geometry induced by the kernel and realize a finite-dimensional approximation of the underlying RKHS. Unlike contrastive objectives, this approach enforces global consistency with the semantic structure rather than only relative discrimination (Zbontar et al., 2021).

3.2. Neural architectures and projection heads for symbolic representation

In modern self-supervised contrastive learning frameworks such as SimCLR (Chen et al., 2020), BYOL (Grill et al., 2020), MoCo v2 (Liu et al., 2024), decoupling structural encoding from metric alignment is an established strategy. These frameworks typically employ a deep backbone for syntax-aware feature extraction and a learnable projection head to map these features onto a target latent space for metric comparisons. Inspired by these techniques, we adopt a similar separation to align neural structural representations with the continuous semantic geometry induced by the robustness kernel, ensuring the backbone retains logical compositionality while the projection enforces semantic consistency.

4. Methodology

Our goal is to learn a neural encoder $f_\theta : \mathcal{F} \rightarrow \mathbb{S}^{D-1}$, where D is the dimensionality of the embedding space, that maps STL specifications $\varphi_i, \varphi_j \in \mathcal{F}$ to latent representations e_i, e_j , such that their dot product approximates the STL kernel similarity from Equation 1:

$$\langle e_i, e_j \rangle \cong k(\varphi_i, \varphi_j)$$

Although the kernel $k(\cdot, \cdot)$ implicitly defines a mapping into a (theoretically) infinite-dimensional RKHS, the encoder $f_\theta(\cdot)$ learns a finite D -dimensional representation that approximates the pairwise semantic relationships of this space. This is achieved via a *weighted geometric alignment loss* (see Section 4.1), promoting semantic agreement under the STL kernel. As a result, formulae with high semantic similarity are encouraged to

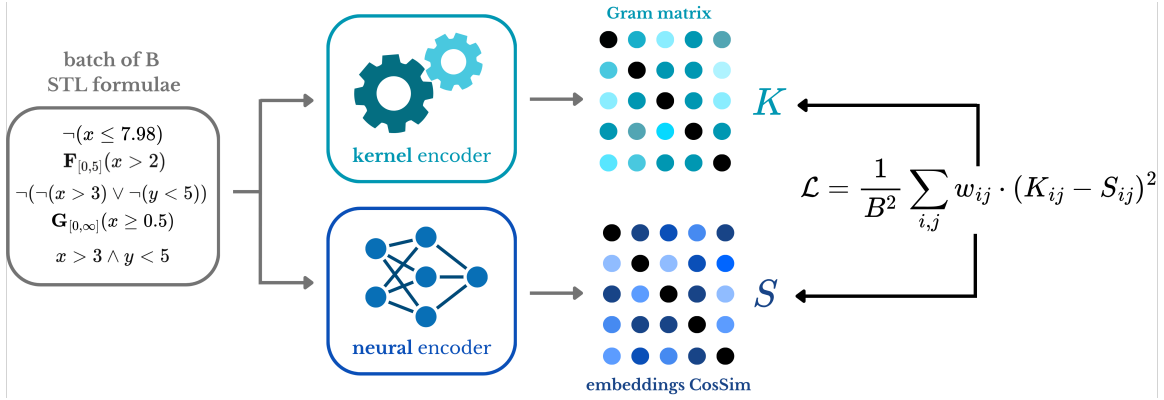


Figure 1: An overview of our proposed approach to distill robustness semantics from a symbolic STL kernel into a Transformer-based encoder for efficient inference.

lie close on the hypersphere, while semantically dissimilar ones are driven toward near-orthogonal positions.

4.1. Weighted geometric alignment loss

The training process aligns latent representation z of a formula φ produced by a Transformer-based encoder $f_\theta(\cdot)$ with the geometric structure induced by a semantic kernel $k(\varphi, \varphi_{ref})$. Unlike standard contrastive approaches that use binary labels¹, our framework treats the kernel value $K_{ij} = k(\varphi_i, \varphi_j)$ as a continuous target in a regression task.

Given a batch B of formulae, we define the kernel-weighted contrastive loss as:

$$\mathcal{L} = \frac{1}{B^2} \sum_{i=1}^B \sum_{j=1}^B w_{ij} \cdot (K_{ij} - S_{ij})^2$$

where $K_{ij} = k(\varphi_i, \varphi_j) \in [0, 1]$ is the STL kernel similarity, and $S_{ij} = \langle e_i, e_j \rangle$ is the dot product between the L_2 -normalized embeddings $e = f_\theta(\varphi) / \|f_\theta(\varphi)\|$.

While cosine similarity S_{ij} lies in $[-1, 1]$, the kernel K_{ij} is non-negative (2.2, Appendix A). This apparent discrepancy is resolved geometrically: pairs of semantically unrelated formulae ($K_{ij} \approx 0$) are driven toward orthogonality on the hypersphere ($S_{ij} \approx 0$), resulting in maximum logical disagreement corresponding to null similarity. This ensures the latent geometry remains consistent with the probabilistic agreement formulation of the STL kernel.

The weight w_{ij} serves as a dynamical focal mechanism, prioritizing pairs in which the Transformer’s structural understanding deviates most from the kernel semantics:

$$w_{ij} = \min \left(\frac{|K_{ij} - S_{ij}|^\gamma}{\mathbb{E}_{i,j \in B} [|K_{ij} - S_{ij}|^\gamma]}, C \right)$$

$|K_{ij} - S_{ij}|^\gamma$ amplifies the gradient for pairs exhibiting high semantic misalignment, while $\mathbb{E}_{i,j \in B} [|K_{ij} - S_{ij}|^\gamma]$ normalizes this quantity relative to the current batch average

1. Pairs are either positive if they match or negative if they do not.

error, stabilizing the learning signal. The clamping operation caps the maximum allowed influence of any pair to a constant C , preventing gradient instabilities for outlier values. The parameter γ controls the focal mechanism, with high values forcing the encoder to converge faster on challenging pairs. The weighting does not affect the target geometry but modulates gradient allocation during training.

4.2. Encoder module

The encoder $f_\theta(\varphi)$ maps discrete STL syntax into a continuous latent space using a deep Transformer-based feature extractor and a non-linear MLP projection head.

Transformer encoder To capture the hierarchical and long-range dependencies inherent in STL specifications, we employ a 12-layer Transformer with 16 attention heads per layer. Since the semantics of STL formulae depend on hierarchical structures, we employ learned positional embeddings to encode the relative precedence of operators. This allows the model to effectively distinguish permutations with identical symbols but different semantics.² Conversely, the model should remain invariant to permutations that preserve semantics, such as the commutativity of logical operators.

Pooling Transformer-based classifiers typically use special designated tokens (e.g., [CLS] or [BOS]) trained end-to-end to aggregate sequence information into a bottleneck representation (Devlin et al., 2019; Radford and Narasimhan, 2018; Reimers and Gurevych, 2019). We evaluate three pooling strategies to summarize the Transformer’s output before passing it to the final projection: mean, [CLS] and [BOS] pooling (2.4).

Concretely, let $H \in \mathbb{R}^{N \times D}$ denote the sequence of hidden states from the final Transformer layer where N is the sequence length and D is the embedding dimension, and $M \in \{0, 1\}^N$ the binary attention mask. For [CLS] and [BOS] pooling, the representation is directly taken from the first token. For mean pooling, the attention mask is used to ensure only valid token positions are included, ignoring padding.

$$e_{[\text{CLS}]} = e_{[\text{BOS}]} = H_1 \in \mathbb{R}^D, \quad e_{\text{mean}} = \frac{\sum_{i=1}^N H_i \cdot M_i}{\sum_{i=1}^N M_i} \in \mathbb{R}^D \quad (2)$$

MLP projector The embedding e pooled using one of the above strategies is mapped to the final latent manifold \mathcal{Z} via a two-layer MLP with a bottleneck architecture:

$$z = \text{MLP}(e) = W_2 \cdot \text{LayerNorm}(\sigma(W_1 \cdot e + b_1)) + b_2,$$

where σ is the GELU activation function (Hendrycks and Gimpel, 2016), providing smooth non-linearities well-suited to the continuous gradients of STL robustness.

The first linear layer $W_1 \in \mathbb{R}^{D \times D/2}$ projects the $D = 1024$ -dimensional input to a $D/2 = 512$ -dimensional bottleneck, forcing the encoder to compress information needed to reproduce the STL kernel similarities and hence promoting the filtering of irrelevant details while retaining semantic structure. Layer Normalization (LayerNorm) is applied to stabilize the feature distribution before the final projection.

2. For example, **always eventually** φ means that φ will happen *infinitely often* (recurrence), while **eventually always** φ means that φ will be *always true from a certain point on* (persistence).

The second layer $W_2 \in \mathbb{R}^{D/2 \times D}$ maps back to the target embedding dimension, and the output is L_2 -normalized onto the unit hypersphere \mathbb{S}^{D-1} :

$$e = \frac{z}{\|z\|} = \frac{f_\theta(\varphi)}{\|f_\theta(\varphi)\|}.$$

Constraining e to the manifold $\mathcal{Z} \subset \mathbb{S}^{D-1}$ ensures that the dot product $\langle e_i, e_j \rangle$ directly computes the cosine similarity between formulae, allowing the latent space to faithfully encode the quantitative kernel semantics. At the same time, the hyperspherical geometry prevents collapse of the embedding space and promotes uniform utilization of all dimensions, maintaining expressive capacity while preserving semantic relationships.

5. Experimental setup

Dataset composition The training and test sets are derived from the seeds in [Candussio et al. \(2025\)](#) through the augmentation pipeline detailed in Appendix B. For each seed formula, we generate: (i) lexically complex formulas with equivalent semantics (10.4%), (ii) parametric perturbations altering numerical values of thresholds and temporal bounds while keeping structure (43.4%), and (iii) hybrid items combining structural and semantic changes (45.7%). This stratification ensures the model learns to capture semantic similarity across varying syntactic and quantitative modifications, resulting in a total of 3.3M formulae.

Training setup The architecture described in Section 4 is trained using the kernel-alignment loss (Section 4.1). Optimization is performed with AdamW ([Loshchilov and Hutter, 2017](#)) at a learning rate of $1 \cdot 10^{-5}$, using `bf16` mixed-precision and gradient accumulation over 4 steps, resulting in an effective batch size of 512. Formulae are tokenized as in [Candussio et al. \(2025\)](#)³, with a maximum sequence length of 512 tokens.

The STL semantic kernel is computed online per mini-batch during the forward pass, avoiding the prohibitive memory overhead of pre-computing a full Gram matrix while allowing the loss to operate on the current embeddings. Training is conducted for 5 epochs, while monitoring the kernel alignment and embedding distribution on the hypersphere.

Training metrics We quantify the quality of learned representations by measuring their faithfulness in reproducing the semantic STL kernel geometry. Since the kernel induces an inner product in the Hilbert space (Section 2.2), a correct embedding should preserve both pairwise similarities and the global distribution of representations. We report three complementary metrics: the kernel-weighted semantic loss (Section 4.1), *kernel alignment*, and embeddings’ *uniformity*. Kernel alignment is the cosine similarity between the vectorized kernel and the neural similarity matrices, ranging from 0 to 1, with higher values indicating better preservation of semantic structure. Uniformity ([Wang and Isola, 2022](#)) quantifies how well the embeddings are spread on the hypersphere, with values in $[-4, 0]$; 0 indicates complete collapse, whereas -4 corresponds to maximal uniform distribution and optimal separation of semantic content (see Appendix C for definitions).

3. In the [CLS] scenario, a special control token is added to serve as a representation bottleneck.

6. Results

6.1. Kernel distillation adherence

Using the training metrics defined above, we find that all three pooling strategies (mean, [CLS], and [BOS]) converge to high adherence values, demonstrating the robustness of our proposed distillation framework. Kernel alignment consistently surpasses 0.9 across configurations, indicating that learned representations accurately reflect kernel similarities. We also find that the uniformity metric stabilizes around -3.0, suggesting that formulae embeddings are spread across the hypersphere to avoid dimensional collapse.

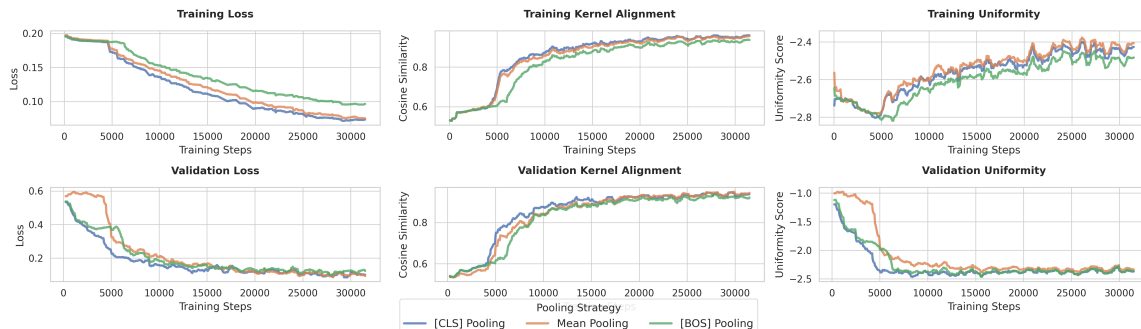


Figure 2: Evolution of training (top) and validation (bottom) metrics over approximately 30,000 training steps for the three pooling strategies ([CLS], mean, and [BOS]).

The left and center panels of Figure 2 illustrate the steady minimization of the geometric alignment loss and the corresponding increase in kernel alignment (> 0.9), demonstrating that the encoder effectively internalizes the target semantic geometry. Validation metrics closely mirror training performance, confirming strong generalization to unseen formulae without syntactic overfitting. The right panels show the uniformity score stabilizing around -2.4 on the validation set, indicating that the representations maintain a well-distributed hyperspherical latent space, avoiding dimensional collapse. Across all configurations, [CLS] pooling (in blue) consistently exhibits the fastest and most stable convergence.

6.2. Semantic agreement

To evaluate whether the trained encoder recovers STL kernel semantics, we compare neural cosine similarity with the corresponding STL kernel value on a test set of logically equivalent formula pairs (≈ 3000 examples). For each pair (φ_1, φ_2) , we compute the mean absolute error (MAE) between the neural and kernel-based metrics, with lower values indicating stronger alignment. As baselines, we employ random formulae from the test set (*Non-equivalent*), as well as lexically similar but semantically distinct formulae, i.e. selected by taking those with the smallest Edit distance and kernel similarity < 0.7 (*Lexically Sim.*). Both neural and kernel distances are normalized by their respective maximum values for intuitive comparison across formula categories.

As shown in Table 1, the model assigns high similarity to equivalent pairs (0.966) and low similarity to non-equivalent ones (0.182). Crucially, it resists *Lexically Sim.* hard negatives

Table 1: Semantic agreement evaluation for [CLS] pooling.

Metric	Equivalent	Non-equivalent	Lexically Sim.
Neural similarity	0.966	0.182	0.308
Kernel similarity	0.997	0.170	0.225
MAE (semantic gap)	0.034	0.072	0.112
Relative neural distance	0.137	0.833	0.770
Relative kernel distance	0.105	0.830	0.775

(0.308), proving that the encoder successfully maps discrete syntax into a continuous space that faithfully reflects true logical semantics.

6.3. Efficiency analysis

We measure the *embedding time* for computing a vector representation for each formula, and the *similarity time* for comparing two embedded formulae, capturing different scalability properties for similarity measurements.

Embedding time The STL kernel has complexity $\mathcal{O}(BNP)$, where B is the number of formulae, N is the number of signals in Monte Carlo evaluation, and $P = 1000$ the number of estimation points (Appendix A). The neural encoder complexity is $\mathcal{O}(BL^2)$, where L is the fixed sequence length. While these trends follow directly from the theoretical complexities, results in Table 2 show that the kernel’s memory footprint grows linearly with NP , whereas Transformer embeddings remain invariant to NP and demonstrate substantial gains in both runtime and memory efficiency across all tested signal counts (as shown in Appendix D).

Table 2: Embedding efficiency comparison ($B = 2000$) on a NVIDIA A100 80GB GPU. **loaded**: inference time for a pre-loaded model; **full** also includes model loading.

Metric	Kernel						Transformer	
	$N = 500$	1000	2000	4000	8000	16000	loaded	full
Time (s)	2.18	3.03	4.77	8.36	17.08	48.86	2.17	3.56
RAM (GB)	4.91	8.74	16.46	31.70	62.38	123.38	1.54	1.71

Pairwise similarities computation Computing pairwise similarities over a batch of B formulae requires constructing a $B \times B$ matrix. However, the computational cost per entry differs substantially. The STL kernel requires computing inner products between robustness vectors over N sampled signals, each with P points, yielding a $\mathcal{O}(B^2NP)$ complexity. In contrast, the neural encoder produces fixed-dimensional embeddings $e \in \mathbb{S}^{D-1}$, and pairwise similarities reduce to a single matrix multiplication, with complexity $\mathcal{O}(B^2D)$ and efficient GPU implementation. Since typically $D \ll N \cdot P$, the neural approach yields significantly lower latency despite the same quadratic scaling in B (see Figures of Appendix D).

6.4. Probing average robustness and satisfaction

To verify that the learned embeddings capture quantitative STL semantics beyond structural cues, we freeze the encoder and train a lightweight regressor on top of the L_2 -

normalized representations to predict two scalar quantities for each formula φ : the average robustness $\bar{\rho}(\varphi)$ and the satisfaction probability $p_{\text{sat}}(\varphi)$, both computed over 1000 signals sampled from a fixed probability distribution μ_0 on trajectories. As a reference, we repeat the same experiment using rows of the STL kernel Gram matrix as input features. In both settings, we train the same two-layer MLP with MSE loss, ensuring architectural symmetry between neural and kernel-based representations⁴. Evaluation on unseen formulae is performed using both Pearson correlation r and mean absolute error (MAE) where the predicted values, where the predicted values \hat{y} are the outputs of a lightweight probe MLP applied to the embeddings, and the true targets y are the quantities computed from 1000 sampled signals per formula: the average robustness $\bar{\rho}(\varphi)$ or the satisfaction probability $p_{\text{sat}}(\varphi)$. The neural embeddings achieve $r = 0.910$ and $\text{MAE} = 0.399$ for robustness, and $r = 0.947$ and $\text{MAE} = 0.062$ for satisfaction, compared to $r = 0.999$ and $\text{MAE} = 0.064$, and $r = 0.994$ and $\text{MAE} = 0.023$ obtained using kernel features. The high correlations and low MAE indicate that the learned embedding space preserves most of the STL quantitative semantics while providing a substantially more compact and efficient representation.

6.5. Decoding neural embeddings

To address the embedding inversion problem (Section 2.3), we investigated whether original symbolic formulae can be reconstructed directly from our frozen neural representations using a decoder-only Transformer analogous to that of Candussio et al. (2025). To explicitly test the structural and semantic richness of the learned latent space, we deliberately restricted the decoder’s training to 5 epochs.⁵ If the continuous embedding faithfully captures the formulae semantics, a downstream decoder should require a significantly reduced training budget to perform the inversion. As in previous sections, we measure the semantic discrepancy between original and decoded formulae from their *robustness vectors* $\rho(\varphi) \in \mathbb{R}^M$, computed by taking a set of M signals $\Xi = \{\xi_i\}_{i=1}^M$ sampled from μ_0 as $\rho(\varphi)_i = \rho(\varphi, \xi_i)$. Intuitively, if the robustness vectors of two formulae are similar, it means that the specifications behave similarly on the trajectories in Ξ , providing a fast approximation of the semantic similarity between formulae. Even under our strict computational budget, the decoder trained on frozen representations achieved a median cosine similarity of 0.8688 and an L_2 -distance of 2.1766. For reference, the Candussio et al. (2025) baseline reports median cosine 0.926–0.985 and median L_2 -distance 12–28. Despite the smaller distance due to different scaling, the high cosine similarity shows that our embeddings capture most semantic information, enabling efficient inversion with far fewer training steps than the baseline.

7. Conclusions

In this work, we present a framework to distill the semantics of robustness-based kernels into Transformer-based models, and demonstrate its application to Signal Temporal Logic (STL) formulae. While standard kernels provide accurate behavioural comparisons, they are computationally intensive, anchor set-dependent, and inherently non-invertible. We

4. This baseline differs from classical kernel ridge regression, as we apply a parametric regressor to kernel-derived features rather than solving the closed-form RKHS regression problem.

5. This corresponds to a quarter of the reference baseline by Candussio et al. (2025).

show that our procedure instead produces embeddings that faithfully preserve semantic similarity at a fraction of the runtime cost.

We also demonstrate that the resulting embeddings are not only semantically rich but also invertible: a decoder used to invert kernel embeddings can rapidly learn to reconstruct original formulae from the distilled latent space, showing that the embedding captures rich structural and semantic information about the underlying logic. Overall, our framework provides a practical and scalable method for reasoning over STL specifications, bridging formal symbolic representations and continuous vectorial embeddings, while preserving the ability to perform formula comparison, retrieval, and reconstruction. Future work will investigate extending this distillation approach to diverse string-based kernels, broadening its scope beyond temporal logics to test the generality of our approach.

References

- Takumi Akazaki, Shuang Liu, Yoriyuki Yamagata, Yihai Duan, and Jianye Hao. *Falsification of Cyber-Physical Systems Using Deep Reinforcement Learning*, page 456–465. Springer International Publishing, 2018. ISBN 9783319955827. doi: 10.1007/978-3-319-95582-7_27. URL http://dx.doi.org/10.1007/978-3-319-95582-7_27.
- Miltiadis Allamanis, Marc Brockschmidt, and Mahmoud Khademi. Learning to represent programs with graphs, 2018. URL <https://arxiv.org/abs/1711.00740>.
- Alain Berlinet and Christine Thomas-Agnan. *Reproducing Kernel Hilbert Space in Probability and Statistics*. 01 2004. ISBN 978-1-4613-4792-7. doi: 10.1007/978-1-4419-9096-9.
- Giuseppe Bombara and Calin Belta. Offline and online learning of signal temporal logic formulae using decision trees. *ACM Trans. Cyber-Phys. Syst.*, 5(3), March 2021. ISSN 2378-962X. doi: 10.1145/3433994. URL <https://doi.org/10.1145/3433994>.
- Luca Bortolussi, Giuseppe Maria Gallo, Jan Křetínský, and Laura Nenzi. Learning model checking and the kernel trick for signal temporal logic on stochastic processes, 2022. URL <https://arxiv.org/abs/2201.09928>.
- Sara Candussio, Gaia Saveri, Gabriele Sarti, and Luca Bortolussi. *Bridging Logic and Learning: Decoding Temporal Logic Embeddings via Transformers*, page 3–18. Springer Nature Switzerland, September 2025. ISBN 9783032060969. doi: 10.1007/978-3-032-06096-9_1. URL http://dx.doi.org/10.1007/978-3-032-06096-9_1.
- Ting Chen, Simon Kornblith, Mohammad Norouzi, and Geoffrey Hinton. A simple framework for contrastive learning of visual representations. In *Proceedings of the 37th International Conference on Machine Learning, ICML’20*. JMLR.org, 2020.
- Jacob Devlin, Ming-Wei Chang, Kenton Lee, and Kristina Toutanova. Bert: Pre-training of deep bidirectional transformers for language understanding. In *North American Chapter of the Association for Computational Linguistics*, 2019. URL <https://api.semanticscholar.org/CorpusID:52967399>.
- Lijun Dong, Hong Yao, Dan Li, Yi Wang, Shengwen Li, and Qingzhong Liang. Improving graph neural network via complex-network-based anchor structure. *Knowledge-Based Systems*, 233:107528, 2021. ISSN 0950-7051. doi: <https://doi.org/10.1016/j.knosys.2021.107528>. URL <https://www.sciencedirect.com/science/article/pii/S0950705121007905>.
- Georgios E. Fainekos and George J. Pappas. Robustness of temporal logic specifications. In *Proceedings of the First Combined International Conference on Formal Approaches to Software Testing and Runtime Verification, FATES’06/RV’06*, page 178–192, Berlin, Heidelberg, 2006. Springer-Verlag. ISBN 3540496998. doi: 10.1007/11940197_12. URL https://doi.org/10.1007/11940197_12.
- Zhangyin Feng, Daya Guo, Duyu Tang, Nan Duan, Xiaocheng Feng, Ming Gong, Linjun Shou, Bing Qin, Ting Liu, Daxin Jiang, and Ming Zhou. Codebert: A pre-trained model

- for programming and natural languages, 2020. URL <https://arxiv.org/abs/2002.08155>.
- Tianyu Gao, Xingcheng Yao, and Danqi Chen. Simcse: Simple contrastive learning of sentence embeddings, 2022. URL <https://arxiv.org/abs/2104.08821>.
- Jean-Bastien Grill, Florian Strub, Florent Alché, Corentin Tallec, Pierre H. Richemond, Elena Buchatskaya, Carl Doersch, Bernardo Avila Pires, Zhaohan Daniel Guo, Mohammad Gheshlaghi Azar, Bilal Piot, Koray Kavukcuoglu, Rémi Munos, and Michal Valko. Bootstrap your own latent a new approach to self-supervised learning. In *Proceedings of the 34th International Conference on Neural Information Processing Systems, NIPS '20*, Red Hook, NY, USA, 2020. Curran Associates Inc. ISBN 9781713829546.
- Mohammadhosein Hasanbeig, Daniel Kroening, and Alessandro Abate. Deep reinforcement learning with temporal logics. In *International Conference on Formal Modeling and Analysis of Timed Systems*, 2020. URL <https://api.semanticscholar.org/CorpusID:221305630>.
- Dan Hendrycks and Kevin Gimpel. Gaussian error linear units (gelus). *arXiv: Learning*, 2016. URL <https://api.semanticscholar.org/CorpusID:125617073>.
- Geoffrey E. Hinton, Oriol Vinyals, and Jeffrey Dean. Distilling the knowledge in a neural network. *ArXiv*, abs/1503.02531, 2015. URL <https://api.semanticscholar.org/CorpusID:7200347>.
- Corinne Jones, Vincent Roulet, and Zaid Harchaoui. Kernel-based translations of convolutional networks, 2019. URL <https://arxiv.org/abs/1903.08131>.
- Chungpa Lee, Sehee Lim, Kibok Lee, and Jy yong Sohn. On the similarities of embeddings in contrastive learning, 2025. URL <https://arxiv.org/abs/2506.09781>.
- Xiao Li, Cristian-Ioan Vasile, and Calin Belta. Reinforcement learning with temporal logic rewards, 2017. URL <https://arxiv.org/abs/1612.03471>.
- Shipeng Liu, Liang Zhao, Deng feng Chen, and Zhanping Song. Contrastive learning for image complexity representation. *ArXiv*, abs/2408.03230, 2024. URL <https://api.semanticscholar.org/CorpusID:271720179>.
- Ilya Loshchilov and Frank Hutter. Decoupled weight decay regularization. In *International Conference on Learning Representations*, 2017. URL <https://api.semanticscholar.org/CorpusID:53592270>.
- Jamie Mahowald, Brian Bell, Alex Ho, and Michael Geyer. Efficient analysis of the distilled neural tangent kernel. 2026. URL <https://api.semanticscholar.org/CorpusID:285541139>.
- Oded Maler and D. Ničković. Monitoring temporal properties of continuous signals. In *FORMATS/FTRTFT*, 2004. URL <https://api.semanticscholar.org/CorpusID:15642684>.

- Wonpyo Park, Dongju Kim, Yan Lu, and Minsu Cho. Relational knowledge distillation. *2019 IEEE/CVF Conference on Computer Vision and Pattern Recognition (CVPR)*, pages 3962–3971, 2019. URL <https://api.semanticscholar.org/CorpusID:131765296>.
- Alec Radford and Karthik Narasimhan. Improving language understanding by generative pre-training. 2018. URL <https://api.semanticscholar.org/CorpusID:49313245>.
- Vasumathi Raman, Alexandre Donz e, Dorsa Sadigh, Richard M. Murray, and Sanjit A. Seshia. Reactive synthesis from signal temporal logic specifications. In *Proceedings of the 18th International Conference on Hybrid Systems: Computation and Control, HSCC '15*, page 239–248, New York, NY, USA, 2015. Association for Computing Machinery. ISBN 9781450334334. doi: 10.1145/2728606.2728628. URL <https://doi.org/10.1145/2728606.2728628>.
- Nils Reimers and Iryna Gurevych. Sentence-BERT: Sentence embeddings using Siamese BERT-networks. In Kentaro Inui, Jing Jiang, Vincent Ng, and Xiaojun Wan, editors, *Proceedings of the 2019 Conference on Empirical Methods in Natural Language Processing and the 9th International Joint Conference on Natural Language Processing (EMNLP-IJCNLP)*, pages 3982–3992, Hong Kong, China, November 2019. Association for Computational Linguistics. doi: 10.18653/v1/D19-1410. URL <https://aclanthology.org/D19-1410/>.
- Gaia Saveri and Luca Bortolussi. Retrieval-augmented mining of temporal logic specifications from data, 2024. URL <https://arxiv.org/abs/2405.14355>.
- Gaia Saveri, Laura Nenzi, Luca Bortolussi, and Jan Křetínský. stl2vec: Semantic and interpretable vector representation of temporal logic, 2024. URL <https://arxiv.org/abs/2405.14389>.
- Ashish Vaswani, Noam Shazeer, Niki Parmar, Jakob Uszkoreit, Llion Jones, Aidan N. Gomez, Lukasz Kaiser, and Illia Polosukhin. Attention is all you need. In *Neural Information Processing Systems*, 2017. URL <https://api.semanticscholar.org/CorpusID:13756489>.
- Tongzhou Wang and Phillip Isola. Understanding contrastive representation learning through alignment and uniformity on the hypersphere, 2022. URL <https://arxiv.org/abs/2005.10242>.
- Jure Zbontar, Li Jing, Ishan Misra, Yann LeCun, and St ephane Deny. Barlow twins: Self-supervised learning via redundancy reduction. *ArXiv*, abs/2103.03230, 2021. URL <https://api.semanticscholar.org/CorpusID:232110471>.

Appendix A. Kernel Implementation and STL Semantics

A.1. Kernel Implementation

The semantic inner product defined in Section 2.2 involves an integral over the signal space \mathcal{T} with respect to the measure μ_0 . In practice, this distance in the semantic space is approximated via Monte Carlo sampling over a set of n stochastic signals $\{\varepsilon_1, \dots, \varepsilon_n\} \sim \mu_0$:

$$\langle \rho(\varphi_i, \cdot), \rho(\varphi_j, \cdot) \rangle_{\mu_0} \approx \frac{1}{n} \sum_{t=1}^n \rho(\varphi_i, \varepsilon_t) \cdot \rho(\varphi_j, \varepsilon_t)$$

To ensure scale invariance, the original formulation considers the cosine similarity of the robustness features in place of their plain dot product. Let $\|\cdot\|$ denote the L_2 -norm in the Hilbert space induced by μ_0 ; the normalized similarity $k'(\cdot, \cdot)$ is computed as:

$$k'(\varphi_i, \varphi_j) = \frac{\langle \rho(\varphi_i, \cdot), \rho(\varphi_j, \cdot) \rangle_{\mu_0}}{\|\rho(\varphi_i, \cdot)\| \cdot \|\rho(\varphi_j, \cdot)\|} \approx \frac{\sum_{t=1}^n \rho(\varphi_i, \varepsilon_t) \cdot \rho(\varphi_j, \varepsilon_t)}{\sqrt{\sum_{t=1}^n \rho(\varphi_i, \varepsilon_t)^2} \cdot \sqrt{\sum_{t=1}^n \rho(\varphi_j, \varepsilon_t)^2}}$$

Finally, the similarity is projected into a Radial Basis Function (RBF) space through an exponential transformation. This maps the angular distance between formulae into a continuous spectrum $k(\cdot, \cdot) \in [0, 1]$:

$$k(\varphi_i, \varphi_j) = \exp\left(-\frac{2 - 2 \cdot k'(\varphi_i, \varphi_j)}{2\sigma^2}\right)$$

The bandwidth parameter σ^2 (set by default to 0.2) controls the resolution of the semantic manifold. Lower values of σ^2 increase the "sharpness" of the kernel, assigning high similarity scores only to formulae that exhibit near-identical behaviour over the sampled trajectories.

A.2. Boolean and Quantitative Semantics of STL

Let $\xi : [0, T] \rightarrow \mathbb{R}^n$ be a trajectory and φ an STL formula. STL admits two complementary semantics:

Boolean semantics The formula φ is satisfied by ξ at time t if $\xi \models_t \varphi$. For an atomic predicate $\mu = x_i \geq \theta$:

$$\xi \models_t \mu \Leftrightarrow x_i(t) \geq \theta.$$

Boolean connectives and temporal operators are interpreted in the standard way:

$$\begin{aligned} \xi \models_t \neg\varphi &\Leftrightarrow \xi \not\models_t \varphi, \\ \xi \models_t \varphi_1 \wedge \varphi_2 &\Leftrightarrow \xi \models_t \varphi_1 \text{ and } \xi \models_t \varphi_2, \\ \xi \models_t \varphi_1 \vee \varphi_2 &\Leftrightarrow \xi \models_t \varphi_1 \text{ or } \xi \models_t \varphi_2, \\ \xi \models_t \mathbf{F}_{[a,b]}\varphi &\Leftrightarrow \exists t' \in [t+a, t+b] : \xi \models_{t'} \varphi, \\ \xi \models_t \mathbf{G}_{[a,b]}\varphi &\Leftrightarrow \forall t' \in [t+a, t+b] : \xi \models_{t'} \varphi. \end{aligned}$$

Quantitative semantics (robustness) The robustness $\rho(\varphi, \xi, t) \in \mathbb{R}$ measures the degree of satisfaction:

$$\begin{aligned} \rho(\mu, \xi, t) &= x_i(t) - \theta, & \rho(\neg\varphi, \xi, t) &= -\rho(\varphi, \xi, t), \\ \rho(\varphi_1 \wedge \varphi_2, \xi, t) &= \min(\rho(\varphi_1, \xi, t), \rho(\varphi_2, \xi, t)), & \rho(\varphi_1 \vee \varphi_2, \xi, t) &= \max(\rho(\varphi_1, \xi, t), \rho(\varphi_2, \xi, t)), \\ \rho(\mathbf{F}_{[a,b]}\varphi, \xi, t) &= \max_{t' \in [t+a, t+b]} \rho(\varphi, \xi, t'), & \rho(\mathbf{G}_{[a,b]}\varphi, \xi, t) &= \min_{t' \in [t+a, t+b]} \rho(\varphi, \xi, t'). \end{aligned}$$

We write $\rho(\varphi, \xi) := \rho(\varphi, \xi, 0)$ when evaluating at $t = 0$. Positive robustness implies satisfaction, negative robustness implies violation, and the magnitude quantifies the distance from the satisfaction boundary.

Appendix B. Dataset Construction

To ensure the training and testing datasets effectively stress the encoder’s recursive understanding, we employed an object-based augmentation strategy acting directly on the Signal Temporal Logic (STL) Abstract Syntax Tree (AST).

Semantic-preserving recursive augmentation pipeline The core of the strategy is a stochastic priority cascade operating on AST nodes. For each node, a transformation is selected based on the probability distribution $P(\cdot)$ detailed in Table 3. To ensure structural complexity, the pipeline implements a forcing loop: if a generated variant does not reach *at least the target minimum depth* (set to $d \geq 5$), the augmentation is re-attempted until the complexity threshold is met.

Table 3: Semantic-preserving augmentation rules. Notation: \square (always), \diamond (eventually), \mathcal{U} (until).

Rule	$P(\cdot)$	Mathematical Transformation
Not-injection	0.1%	$\varphi \rightarrow \neg\neg\varphi$ (if parent $\neq \neg$)
De Morgan rewriting	9.9%	$(A \wedge B) \rightarrow \neg(\neg A \vee \neg B)$ (and dual)
Time partitioning	35.0%	$\text{op}_I\varphi \rightarrow \text{op}_{I_1}(\text{op}_{I_2}\varphi)$, $\text{op} \in \{\square, \diamond\}$
Until nesting	25.0%	$\varphi \rightarrow (\varphi\mathcal{U}\psi)$ or $(\psi\mathcal{U}\varphi)$
Temporal identity	5.0%	$\varphi \rightarrow \text{op}_{[0,0]}\varphi$, $\text{op} \in \{\square, \diamond\}$
Distributivity	15.0%	$\square_I(A \wedge B) \rightarrow \square_I A \wedge \square_I B$ (or dual)
Predicate inversion	8.0%	$x_i \leq \theta \rightarrow \neg(x_i > \theta)$
<i>No change (default)</i>	2.0%	$\varphi \rightarrow \varphi$

Semantic-altering perturbations The pipeline generates variants through a **stratified approach**. While some variants only undergo structural complication, 65% of the dataset is subjected to semantic shifts that move the satisfaction boundaries. These shifts are applied orthogonally to the structural transformations: a formula may first be logically complicated

to reach the target depth and subsequently perturbed numerically. Perturbations are equally split ($P = 0.5$) between:

- **Vibration:** multiplicative noise affecting thresholds ($\pm 10\%$) and time bounds ($W' \in [0.6 \cdot W, 1.8 \cdot W]$).
- **Shift:** additive offsets ($\Delta \in [-6, 6]$ for thresholds, $\Delta \in [-15, 40]$ for time bounds).

This layering ensures that semantically distinct formulae still retain the high syntactic complexity required to stress the encoder.

Post-serialization refinement Once serialized, three final operations de-correlate surface syntax from logic and ensure formula integrity:

- **Duality shift (40% probability):** Temporal operators are replaced with their negated duals via regex-based substitution: $\Box_{[I]}A \iff \neg\Diamond_{[I]}\neg A$.
- **Interval consistency:** The algorithm strictly enforces the temporal constraint $R > L$. Following any perturbation, the upper bound is reset as $R' = L' + W'$, where the new width W' is sampled stochastically.
- **Empirical validation:** Every formula variant is evaluated against a stochastic dummy signal. This ensures the formula is compatible with the signal’s temporal horizon and does not result in undefined robustness values or empty traces due to excessive nesting or parameter shift.

Appendix C. Training metrics in detail

In our setting, **kernel alignment** quantifies the global agreement between the semantic similarity induced by the STL kernel matrix $K \in \mathbb{R}^{B \times B}$ and the neural similarity matrix $S \in \mathbb{R}^{B \times B}$ obtained from the learned embeddings.

Denoting by $\text{vec}(\cdot)$ the flattening operator, we define:

$$\text{kernel_alignment}(K, S) = \frac{\text{vec}(K) \cdot \text{vec}(S)}{\|\text{vec}(K)\|_2 \cdot \|\text{vec}(S)\|_2}.$$

This quantity corresponds to the cosine similarity between the two vectorized Gram matrices. An alignment value of 1.0 flags that the learned embedding preserves all pairwise inner products up to a global scaling factor, meaning that the neural representation approximates the geometry of the STL semantic Hilbert space⁶.

Uniformity measures how the representations are distributed on the unit hypersphere and serves as a safeguard against representational collapse. Even if pairwise similarities are locally preserved, the embedding may degenerate by concentrating most formulae in a restricted region of the space, reducing the expressive capacity of the representation.

6. While Wang and Isola (2022) defines alignment over discrete positive pairs, our formulation generalizes the concept to a continuous similarity structure, reflecting the graded notion of semantic agreement induced by STL robustness.

Following Wang and Isola (2022), uniformity is defined as the logarithm of the average Gaussian potential over all pairs in the batch:

$$\mathcal{U}(Z) = \log(\mathbb{E}_{i,j \in B} [\exp(-2\|z_i - z_j\|_2^2)]).$$

This formulation corresponds to the case $t = 2$ in Wang and Isola (2022). High uniformity indicates that the embedding occupies the hypersphere broadly, ensuring that semantically distinct specifications are mapped to separable regions of the latent space and preventing many-to-one semantic collapse. Its values range in the extremes $[-4, 0]$ and can be briefly interpreted as follows:

$\mathcal{U}(Z)$	geometrically	interpretation
0.0	complete collapse	zero discriminative power; all formulae are isomorphic
-1.0	dense clustering	poor resolution; distinct logics occupy overlapping regions
-2.5	reasonable distribution	reliable separation of standard temporal properties
-3.0	good sparsity	maximum entropy; preserves fine-grained semantic nuances.
-4.0	asymptotic limit	theoretical maximum spread for $d \rightarrow \infty$ with $t = 2$

The **upper bound** means complete dimensional collapse since it only happens whether all the embeddings exhibit zero euclidean distance, i.e.

$$\|z_i - z_j\|_2^2 = 0, \quad \forall i, j \in B$$

This would cause the uniformity to be null:

$$\mathcal{U}(Z) = \log(\mathbb{E}_{i,j \in B} [\exp(-2 \cdot 0^2)]) = \log(\mathbb{E}_{i,j \in B} [\exp(0)]) = \log(1) = 0$$

thus we can only observe zero uniformity when the model is unable to discriminate between different formulae, neither in syntactical or in semantic terms.

On the opposite, the *theoretical lower bound* corresponds to a perfectly uniform distribution of points across the hypersphere. Formally, for an infinite number of formulae distributed uniformly according to the surface area measure σ_d , the uniformity becomes:

$$\mathcal{U}(Z) = \log \int_{\mathcal{S}^{d-1}} \int_{\mathcal{S}^{d-1}} \exp(-2 \cdot \|u - v\|_2^2) d\sigma_d(u) d\sigma_d(v)$$

where $\|u - v\|_2^2 = \|u\|_2^2 + \|v\|_2^2 - 2u^T v = 2 - 2u^T v$ since $u, v \in \mathcal{S}^{d-1}$. Thus, the expression reduces to:

$$\mathcal{U}(Z) = -2 \cdot 2 + \log \mathbb{E}_{u,v \sim \sigma_d} [\exp(2 \cdot 2u^T v)]$$

As the dimension $d \rightarrow \infty$, $u^T v \rightarrow 0$, leading the (empirical) lower bound to:

$$\mathcal{U}(Z) = -4 + \log \mathbb{E}_{u,v \sim \sigma_d} [\exp(0)] = -4 + \log(1) = -4$$

Appendix D. Time and memory details

The benchmarks reported in Tables 4 and 5 were collected to compare the STL kernel and the Transformer-based model. Both approaches were evaluated on the same dataset of STL

formulae and synthetic signals, ensuring comparability. Memory usage accounts for both CPU RAM and GPU VRAM, capturing peak consumption during embedding and similarity computation stages.

The selection of formulae is deterministic: for each benchmark run, the first B elements of the dataset are taken and used for computation. No random sampling is performed at this stage, ensuring reproducibility across runs. Each formula is then processed either through the Transformer-based embedding pipeline or via the STL kernel approach. For the *Transformer* pipeline, each formula is tokenized using its tokenizer and forwarded through the trained model to extract embeddings. Formulae were tokenized in batches using a multithreaded DataLoader, and embeddings were extracted via forward passes without gradient computation. Similarity matrices were computed using normalized inner products of embeddings. Memory usage is monitored separately for RAM and VRAM, and timing is measured using GPU-synchronized timers to ensure precise measurement of both the forward pass and similarity computations. Benchmarks are repeated for two scenarios: one where the model is already loaded, and one including the full model loading. For the *STL kernel* approach, synthetic signals are first sampled to produce N trajectories, each with 1000 points and 3 variables. Formulae are then evaluated over these signals to compute their robustness vectors. The kernel matrix is finally computed as a similarity measure between the robustness vectors. Both memory (RAM + VRAM) and time are recorded, capturing peak consumption during robustness computation and kernel evaluation.

All experiments are run on the same hardware setup (an NVIDIA A100 80GB GPU), ensuring a fair comparison between the two methods. Memory usage includes both CPU RAM and GPU VRAM allocations, measured using system-level queries and PyTorch memory tracking. Timing accounts for all GPU synchronization points to avoid underestimating the actual execution time.

Table 4: Embedding times (s) and total memory usage (MB) for STL kernel and Transformer. Total memory = RAM + VRAM. “Loaded” refers to Transformer with model already initialized; “Full pipeline” includes model loading.

B	N	STL Kernel		Transformer			
		T_{Emb}	Mem	T_{Emb} (Loaded)	Mem (Loaded)	T_{Emb} (Full)	Mem (Full)
500	500	0.61	2059	0.62	2136	2.06	2914
500	1000	0.83	3061	0.62	2128	1.98	2916
500	2000	1.25	5051	0.62	2128	2.05	2918
500	4000	2.21	8955	0.63	2134	2.02	2918
500	8000	4.53	16995	0.62	2127	1.98	2918
500	16000	12.44	32442	0.62	2126	1.99	2918
1000	500	1.09	3027	1.11	2139	2.53	2911
1000	1000	1.54	4960	1.11	2138	2.54	2911
1000	2000	2.40	8829	1.11	2138	2.53	2910
1000	4000	4.63	16505	1.11	2139	2.48	2910
1000	8000	9.10	32008	1.11	2139	2.47	2909
1000	16000	24.70	62338	1.11	2138	2.56	2910
2000	500	2.18	4907	2.17	2158	3.59	2914
2000	1000	3.03	8737	2.16	2151	3.56	2914
2000	2000	4.77	16464	2.18	2155	3.59	2914
2000	4000	8.36	31696	2.15	2156	3.52	2915
2000	8000	17.08	62384	2.16	2152	3.55	2912
2000	16000	48.86	123384	2.17	2143	3.56	2913
4000	500	4.33	8755	4.45	2163	5.91	2992
4000	1000	6.09	16452	4.41	2162	5.84	2988
4000	2000	9.47	31897	4.42	2163	5.88	2985
4000	4000	17.06	62408	4.38	2162	5.86	2986
4000	8000	34.30	123788	4.42	2158	5.84	2980
4000	16000	232.63	246151	4.46	2157	6.20	2980

Computational scaling of the kernel method and the Transformer-based embedding pipeline. Runtime (Figure D) and memory usage (Figure D) are reported as functions of signal resolution N and batch size B . Projected values (dashed) indicate configurations exceeding memory limits (OOM).

Table 5: Pairwise similarity computation times (s) and total memory usage (MB) for STL kernel and Transformer. Total memory = RAM + VRAM. “Loaded” refers to Transformer with model already initialized; “Full pipeline” includes model loading. Kernel hits OOM for large N .

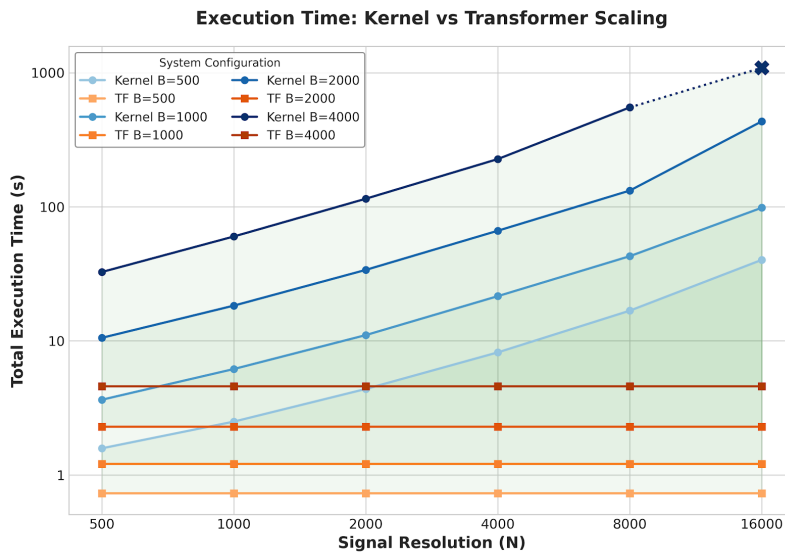
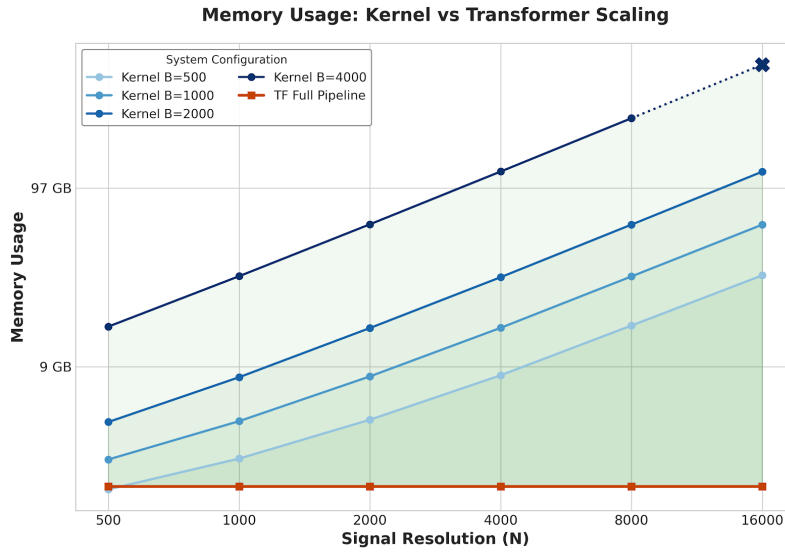
B	N	STL Kernel		Transformer (Loaded)		Transformer (Full)	
		T_{Sim}	Mem	T_{Sim}	Mem	T_{Sim}	Mem
500	500	1.58	2059	0.73	2136	2.04	2914
500	1000	2.50	3061	0.73	2128	1.99	2916
500	2000	4.38	5051	0.73	2128	2.02	2918
500	4000	8.21	8955	0.73	2134	2.02	2918
500	8000	16.81	16995	0.73	2127	1.99	2918
500	16000	40.24	32442	0.73	2126	1.99	2918
1000	500	3.64	3027	1.21	2139	2.52	2911
1000	1000	6.17	4960	1.22	2138	2.53	2911
1000	2000	11.05	8829	1.21	2138	2.52	2910
1000	4000	21.57	16505	1.22	2139	2.47	2910
1000	8000	42.86	32008	1.22	2139	2.45	2909
1000	16000	98.51	62338	1.21	2138	2.56	2910
2000	500	10.54	4907	2.29	2158	3.53	2914
2000	1000	18.33	8737	2.28	2151	3.59	2914
2000	2000	33.87	16464	2.29	2155	3.62	2914
2000	4000	66.37	31696	2.27	2156	3.53	2915
2000	8000	132.29	62384	2.28	2152	3.54	2912
2000	16000	434.57	123384	2.29	2143	3.55	2913
4000	500	32.65	16776	4.59	2163	5.85	2992
4000	1000	60.11	32112	4.55	2162	5.93	2988
4000	2000	114.98	62653	4.53	2155	6.05	2985
4000	4000	227.25	123651	4.51	2156	6.47	2986
4000	8000	552.04	245724	4.58	2152	5.83	2980
4000	16000	1089.28*	489898*	4.65	2152	6.01	2980

Appendix E. [CLS], [BOS] and mean pooling comparison

In Section 4, we introduced three distinct pooling strategies to aggregate the token-level representations produced by the Transformer encoder into a single fixed-dimensional embedding. To evaluate the sensitivity of our distillation framework to the chosen aggregation method, we present a detailed semantic understanding evaluation for each strategy.

Table 1 (reproduced here from the main text for ease of comparison), Table 7, and Table 8 report the performance of [CLS], mean, and [BOS] pooling, respectively. Across all metrics, the results demonstrate that the proposed kernel-alignment objective is highly robust to the choice of pooling operation.

While [CLS] pooling exhibits a marginally tighter alignment with the target kernel similarities (yielding the lowest Mean Absolute Error of 0.034 on equivalent pairs), both



mean and [BOS] pooling successfully internalize the continuous semantic geometry. All three strategies consistently and effectively separate semantically equivalent formulae from non-equivalent and syntactically similar ones. This confirms that the architectural bottleneck effectively compresses logical meaning and filters out syntactic noise, regardless of the specific token aggregation heuristic employed.

Table 6: Semantic understanding evaluation for [CLS] pooling (reference).

Metric	Equivalent	Non-equivalent	Syntactically similar
Neural similarity	0.966	0.182	0.308
Kernel similarity	0.997	0.170	0.225
MAE (semantic gap)	0.034	0.072	0.112
Relative neural distance	0.137	0.833	0.770
Relative kernel distance	0.105	0.830	0.775

Table 7: Semantic understanding evaluation for mean pooling.

Metric	Equivalent	Non-equivalent	Syntactically similar
Neural similarity	0.954	0.201	0.332
Kernel similarity	0.997	0.163	0.221
MAE (semantic gap)	0.044	0.066	0.143
Relative neural distance	0.169	0.833	0.749
Relative kernel distance	0.100	0.837	0.779

Table 8: Semantic understanding evaluation for [BOS] pooling.

Metric	Equivalent	Non-equivalent	Syntactically similar
Neural similarity	0.946	0.171	0.280
Kernel similarity	0.997	0.152	0.182
MAE (semantic gap)	0.052	0.070	0.133
Relative neural distance	0.186	0.834	0.794
Relative kernel distance	0.111	0.848	0.818